DOI 10.24425/aee.2025.153906

Study of power and voltage maps of a tri-stable electromagnetic energy harvester connected to a step-up converter

MARCIN KULIK ✉, KRZYSZTOF GÓRECKI, MARIUSZ JAGIEŁA

Faculty of Electrical Engineering, Automatic Control and Informatics
Opole University of Technology
45-758 Opole, ul. Prószkowska 76
e-mail: {✉ m.kulik/k.gorecki/m.jagiela}@po.edu.pl

(Received: 04.09.2024, revised: 11.05.2025)

Abstract: Due to the specific operation and complex structure of the energy harvesting system, comprising a tri-stable nonlinear vibration energy harvester and a step-up converter, its performance can hardly be represented by a family of curves. For this reason, this paper presents its performance maps determined experimentally. Various converter parameters and loading resistances are used to assess the influence of excitation acceleration on output voltage and power. This study reveals that the system achieves a maximum power of 30.25 mW and a maximum output voltage of 5.32 V at an excitation acceleration of 10 m/s^2 under optimal conditions. The analysis identifies operating regions restricted by the converter parameters where the system attains a minimum applicable voltage between 1.8 and 3.3 V alongside the acceptable output power. This makes it appropriate for powering wireless measurement systems and MEMS devices. The results reveal the need to adjust the converter settings to real-world scenarios adaptively.

Key words: AC/DC step-up converters, bridgeless boost rectifiers, energy harvesting, performance maps, tri-stable electromagnetic converter

1. Introduction

Environmental vibration energy is an omnipresent source for powering wireless measurement systems and MEMS devices. The conversion of mechanical energy through piezoelectric, electromagnetic, and triboelectric transducers has been the focus of extensive scientific research, leading to various vibration energy harvesting (VEH) technologies [1–11]. The use of nonlinear phenomena,

such as bi-stability and tri-stability, allows for a significant increase in the operational bandwidth of energy harvesters compared to linear systems, which is crucial for effectively collecting energy from a wide range of vibration frequencies [1, 2, 4, 5, 12–15]. Introducing additional magnets into energy harvesting systems enables the manipulation of the potential energy characteristics, reducing barriers and facilitating transitions between stable fixed points, leading to increased energy efficiency [6,9]. Therefore, these solutions can be applied to vibration sources with variable frequencies. Studies have shown that these systems can generate significant electrical energy even at low vibration amplitudes, making them attractive for powering wireless sensors and portable devices [8, 10, 11].

The voltage converter is an indispensable component for extracting energy from the generator. Its principal objective is to effectively harvest energy and boost the voltage to levels suitable for recharging the control device's battery. The output voltages from the generator are AC voltages, often in the range of several hundred millivolts. Therefore, this voltage needs to be rectified and increased to values that enable charging the battery to power the entire system. Additionally, the converter should be as compact as possible, and all components should be optimized for energy consumption. Several works present advances in energy harvesting systems, focusing on optimizing and innovating electronic converters for various applications. In work [16], the authors focus on improving rectifier circuits and comparing bridge and dual-voltage configurations to optimize the energy efficiency of piezoelectric systems. Publication [17], on the other hand, introduced a novel AC–DC boost converter using the harvester's coil as a storage element, eliminating external inductors and adapting to random vibration sources for magnetostrictive energy harvesters. Paper [18] presents the design of a low-voltage DC-DC converter tailored for IoT (Internet of things) and on-chip applications, achieving an ultra-low voltage operation through an innovative charge pump topology and an MPPT (Maximum power point tracking) integration. In a publication [19], the authors proposed a hybrid energy harvesting system combining vortex- and gallop-induced oscillations to increase throughput and power generation in wind energy applications. Paper [20] reviewed MPPT techniques, offering insights into their critical role in maximizing the efficiency of energy conversion systems across photovoltaic and piezoelectric domains. All these works underscore the ongoing innovation in electronic converters to address efficiency, adaptability, and sustainability in energy harvesting technologies. Further examples of electronic converters can be found in publications [21–25]. An AC voltage is usually rectified in these solutions first, and then a DC/DC converter boosts the voltage. In publications [26,27], the authors present a solution in which AC voltage is simultaneously boosted and converted to DC voltage without a rectifying bridge (bridgeless boost rectification). These works describe in detail the operating principle of this unique solution, which combines boost and buck-boost converters. Accurate zero-crossing detection of the generated voltage signal is needed for efficient control. The authors in the publication used a combination of an operational amplifier and a comparator. The efficiency of this converter ranges from 40% to over 70%, depending on the generator output voltage. In our research paper, we comprehensively analyzed a tri-stable electromagnetic energy harvester and a bridgeless boost rectifier to meticulously determine the optimal parameters for such a converter, ensuring the utmost efficiency in system operation. The research was conducted based on measurements of the voltage and output power of the entire system. Although the time-domain modeling of the energy harvesters alone is commonly used, accurate, and fast, the time-domain model of the converter, which considers semiconductors and discrete components operating at PWM frequency, would be too complex, leading to unacceptably long calculation times. Therefore, measurements were preferred here over simulations to ensure

reliable conclusions. While the effects of PWM frequency and duty cycle on converter performance have been extensively studied in the literature for more conventional systems [21–27], this research focuses on a tri-stable electromagnetic energy harvester connected to a particular bridgeless boost rectifier. By experimentally mapping the output power and voltage across a wide range of power converter parameters (e.g., PWM frequency, duty cycle, load resistance, and excitation acceleration), we provide implications for the optimization of control of such systems. In our previous work, we developed and patented a vibration energy harvester [28], forming the basis for this study. In subsequent research, we introduced a method for optimizing the system voltage and output power by precisely placing winding turns in the best magnetic coupling region [29]. This significantly improved the system's efficiency. In the next step, we examined the practical applicability of this type of system. A voltage converter was connected to the output of the energy harvester, enabling the generation of DC output voltages exceeding 3 V. Additionally, we investigated the impact of the scale factors on the output parameters of the system, an electronic converter [30].

This work focuses on the experimental analysis of performance maps for a tri-stable electromagnetic energy harvester integrated with a step-up converter. The study mainly aims to understand the influence of key settings of a boost rectifier and loading conditions on system performance. By identifying operating regions delineated by the converter settings where the system achieves minimum proper voltage levels, this research contributes to the practical application of such systems in powering electronic devices with low power demand.

2. Considered harvesting system

This paper analyzes an electromagnetic system for harvesting energy from mechanical vibrations and a voltage converter outlined in [28–30], which is now considered connected to a boost converter. The electrical energy generator alone features the magnetic circuit depicted in Fig. 1. Its operating principle involves inducing a voltage in two coils connected in parallel due to the movement of yokes containing high-energy permanent magnets. These yokes are attached to a bending beam, which transfers and amplifies external vibrations using nonlinear resonance. This system is tri-stable, meaning that the yokes' displacement along the y-axis features three stable points. This is due to the specific action of magnetic force that acts between the moving permanent magnets and the magnets in the support. Thanks to this additional force, the system becomes nonlinear, thereby enabling the generation of electrical voltage across a wider frequency range compared to linear systems (those lacking magnets in the support). This magnetic force can be considered as an additional stiffness force besides the stiffness of the beam alone. Figures 1(b–d) depict the equilibrium points of the system. The balance of internal and external forces of the harvester without a boost converter is as follows:

$$m\frac{\mathrm{d}^2\zeta(t)}{\mathrm{d}t^2} + c\frac{\mathrm{d}\zeta(t)}{\mathrm{d}t} + [k + k_{\mathrm{mag}}(\zeta)]\zeta(t) + F_{\mathrm{e}}(t) = ma_{\mathrm{rms}}\sqrt{2}\sin(2\pi f_{\mathrm{vib}}t) - mg, \tag{1}$$

where: m is the mass of the vibrating part, c is the damping coefficient, k is the cantilever beam stiffness, k_{mag} is the strongly nonlinear stiffness from the magnetic force, which allows one to obtain tri-stable equilibria, ζ stands for the displacement of the vibrating part, a_{rms} is the rms value of excitation acceleration, f_{vib} represents the vibration frequency, F_{e} is the electromagnetic

force, g is the gravity constant, and t is the time. The current through the load can be determined from the equation:

$$\frac{\mathrm{d}i(t)}{\mathrm{d}t} = \frac{e - i(R_\mathrm{L} + R_\mathrm{c})}{L_\mathrm{c}}, \tag{2}$$

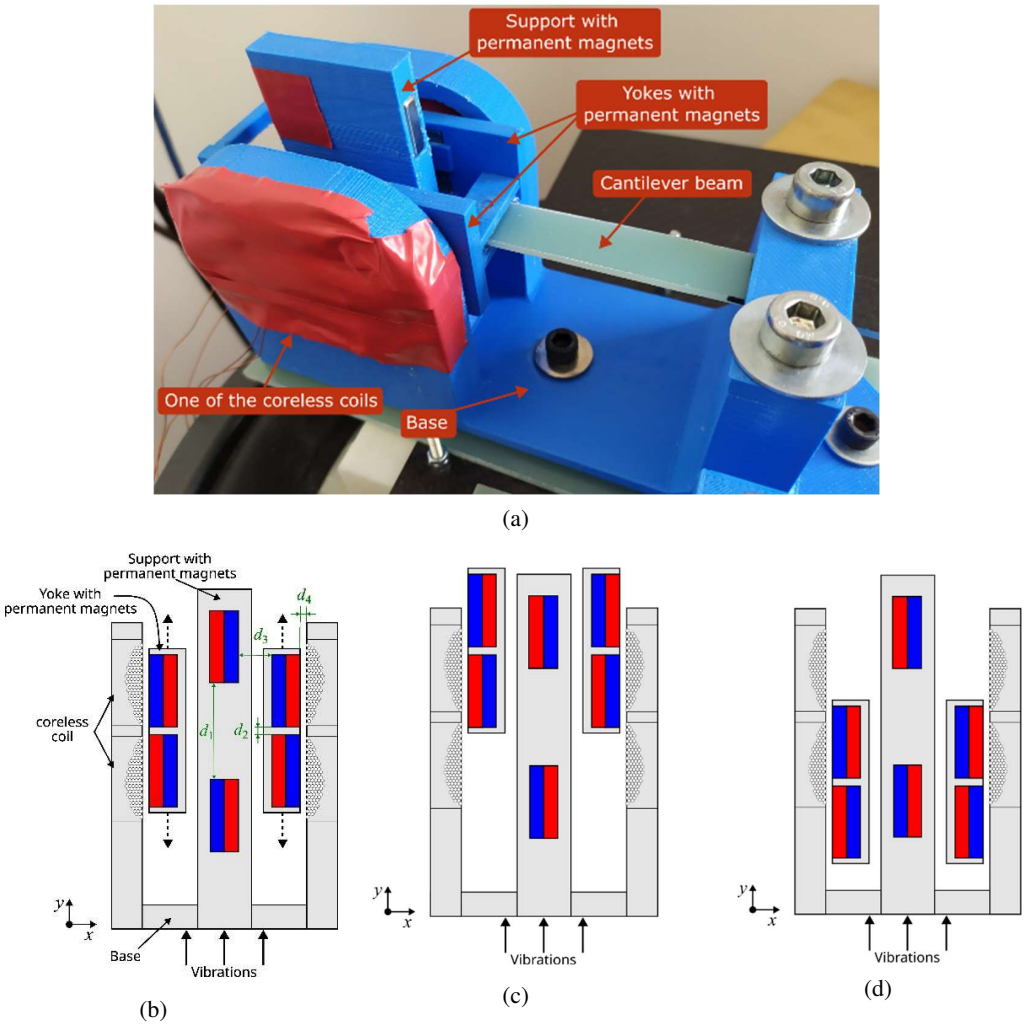

Fig. 1. Electromagnetic vibration energy harvester (a); cross-section of the magnetic circuit of voltage generator at the central equilibrium point of yokes with permanent magnets (b); remaining equilibrium points (c), (d)

where e, R_{L}, R_{c}, L_{c} are the electromotive force, load resistance, coils' resistance and inductance, respectively. The parameters k_{mag}, F_{e} and e can be determined from the formulas:

$$k_{\mathrm{mag}} = \frac{F_{\mathrm{mag}}(\zeta)}{\zeta}, \tag{3}$$

$$F_{\mathrm{e}} = \frac{\mathrm{d}\lambda}{\mathrm{d}\zeta} i(t), \tag{4}$$

$$e = \frac{\mathrm{d}\lambda}{\mathrm{d}\zeta}\frac{\mathrm{d}\zeta}{\mathrm{d}t}, \tag{5}$$

where $F_{\mathrm{mag}}(\zeta)$ is the magnetic force and λ is the flux linkage. Table 1 outlines the dimensions and materials used for the generator components.

Table 1. Dimensions and materials of electromagnetic vibration energy harvester

Component	**Materials**	**Dimensions**
Cantilever beam	Glass-epoxy composite, E = 12.3 GPa, ρ = 2 g/cm^3	(length – width – thickness) 70.3 mm – 15 mm – 2 mm
Coreless coils connected in parallel	Copper Ø 0.5 mm	100 turns, R_c = 0.75 Ω, L_c = 0.0001 H
Magnetic circuit	NdFeB N38, B_r – 1.23 T	Permanent magnets (length in direction $x - y - z$) 5 mm – 15 mm – 40 mm (see Fig. 2(b)) d_1 = 24.5 mm, d_2 = 0.5 mm, d_3 = 5 mm, d_4 = 1 mm

The feature of the electromagnetic vibration energy converters is a low output voltage amplitude. It is imperative to employ a voltage converter to harvest electrical energy for applications such as powering wireless measurement systems or recharging batteries. This converter must exhibit minimal voltage drop during rectification and possess the capability to amplify the voltage to the requisite level of 3.3 V.

A bridgeless boost rectifier (see Fig. 2(a)), as elucidated by the authors in [25, 27], was chosen to operate in conjunction with this transducer. The primary function of this converter is to rectify the voltage by controlling switches S1 and S2 in the upper and lower halves of the sinusoidal signal produced by the generator. The designed circuit for this purpose is depicted in Fig. 2(b). In our solution, a sole comparator is responsible for detecting the signal zero-crossing, which is a simple and efficient solution. The signal originating from the generator is directed toward a low-pass filter, which effectively eliminates the high-frequency component associated with the operation of switches S1 and S2 in the converter. Additionally, a Schottky diode is incorporated at the non-inverting input to accurately discern the signal's polarity utilizing a comparator powered by a single supply voltage. A capacitor is integrated to mitigate potential oscillations at the comparator output. The signal originating from the comparator is directed toward the external interrupt input of the ultra-low-power MSP430FR6922 microcontroller. The average current consumption

of this microcontroller while in active mode operating at 1 MHz is approximately 100 μA. Additionally, through power-conserving modes, the current consumption by the microcontroller can be significantly diminished. This microcontroller plays a crucial role in the possibility of directly switching the transistors that determine the operation of the converter. It also can tune the duty cycle of the pulses D_{PWM}, thus effectively regulating the switches and the frequency f_{PWM} of the produced PWM signal. Generally, the DC components of the output voltage and current of the whole system, hereinafter referred to as the output voltage and current, can be represented, respectively, by the two relationships

$$V_{\mathrm{out}} = f_1(t, V_{\mathrm{out}}, I_{\mathrm{out}}, e\,(a_{\mathrm{rms}}), f_{\mathrm{PWM}}, D_{\mathrm{PWM}}, R_{\mathrm{L}}), \tag{6}$$

$$I_{\mathrm{out}} = f_2(t, V_{\mathrm{out}}, I_{\mathrm{out}}, e\,(a_{\mathrm{rms}}), f_{\mathrm{PWM}}, D_{\mathrm{PWM}}, R_{\mathrm{L}}), \tag{7}$$

where f_1 and f_2 are highly nonlinear implicit functions containing discontinuous variables and both slowly changing and rapidly changing parameters. For this reason, it becomes exceedingly challenging to model accurately. The focus of this study primarily resides in the experimental evaluation of the system performance. Table 2 summarizes the parameters of the prototype converter connected to the generator.

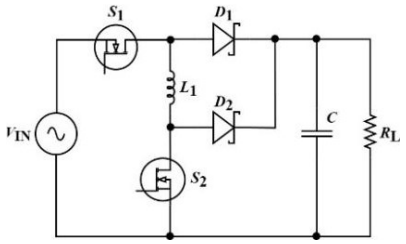

Fig. 2. Bridgeless boost rectifier for energy harvesting (a); zero-crossing detection circuit and control circuit for proposed boost converter (b); manufactured prototype (c); laboratory setup (d)

Table 2. Components and parameters in the prototype

Component	**Parameters**	**Part number**
MOSFETs	20 V, 8 A, 22 mΩ	SI9926CDY
Inductor	10 μH, 5.8 A, 18 mΩ	N/A
Output capacitors	470 μF	EEE1AA471UP
Comparators	–	TLV7012DDFR
Schottky diodes	V_f = 240 mV, 600 mA	BAT54W-HG3-18
Microcontroller	–	MSP430FR6922

Figure 2(c) shows a photo of the prototype converter. The prototype is designed for a dual-power channel version to accommodate the integration of two generators operating in different frequency ranges. However, currently, a single channel is used to examine the performance of a tri-stable system.

3. Maps of output voltage and power

The measurements were conducted on a laboratory setup consisting of a vibration table, an amplifier, an accelerometer, and a computer with a data acquisition card (see Fig. 2(d)). Frequency response characteristics were obtained by measuring the voltage drop across the load during the excitation of the vibration table using a sine test with the frequency backward. The sweep time between frequencies from 35 Hz to 15 Hz was set to 20 seconds. The studies were carried out for two different excitation accelerations, namely 5 m/s^2 and 10 m/s^2. Preliminary measurements were performed only for the generator without the voltage converter. Frequency response characteristics were measured for various loads to examine the voltage and power of the generator. As shown in Fig. 3, the bandwidth where a relatively large voltage (with an amplitude above 0.5 V) is generated significantly depends on the excitation acceleration and the load resistance. The maximum achievable bandwidth occurs at an acceleration of 10 m/s^2 and a load of 20 Ω, approximately 10 Hz. A softening effect can be observed in a system with increasing excitation acceleration. An increase in the yoke displacement amplitude results in a decrease in the effective stiffness of the system due to the presence of magnetic force. As a result of this effect, the resonant frequency shifts towards lower frequencies.

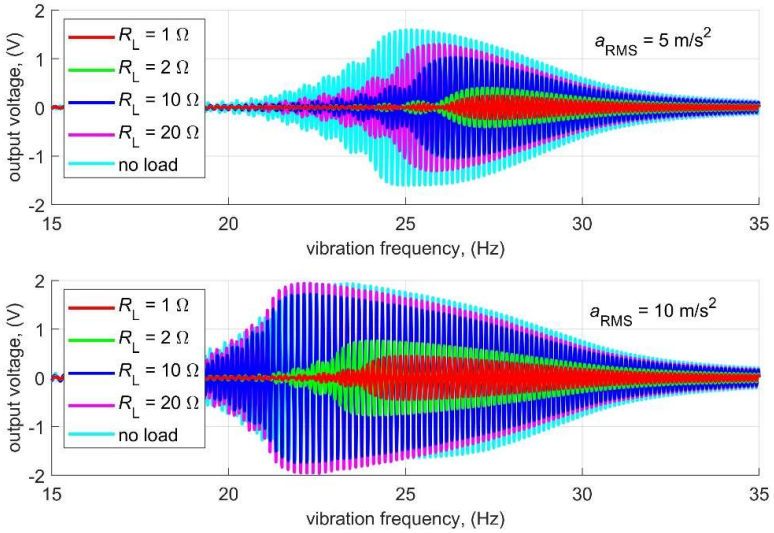

Fig. 3. Measured output voltage for frequency sweep from 35 to 15 Hz and excitation acceleration equal to 5 and 10 m/s^2

Figure 4 shows the power vs. vibration frequency (while decreasing the frequency) as a loading function. The power on the resistive load was determined based on the calculated RMS value from the measured voltage signal. As can be observed, the generated power is tens of milliwatts, with a maximum value of 88 mW at an acceleration of 10 m/s^2 and a load of 2 Ω. The decreasing loading significantly narrows the system's bandwidth due to the interaction of the electromagnetic force of the interaction between the permanent magnets in the yokes and the current through the coils.

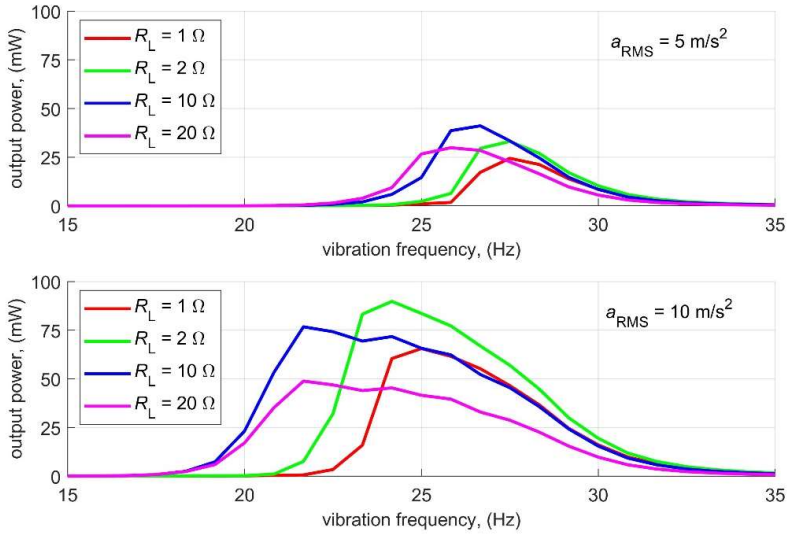

Fig. 4. Measured output power at different loads during a frequency sweep from 35 to 15 Hz, with excitation accelerations of 5 and 10 m/s^2

In the next step, measurements were conducted with the generator connected to the bridgeless boost rectifier (see Fig. 2). For each acceleration value, the influence of converter parameters such as PWM duty cycle, PWM frequency, and load resistance on the voltage and power output of the miniature DC source was examined. An experiment was conducted on a regular grid containing 5^3 points for these three parameters. Based on preliminary measurements, the range of variations for these parameters was established as follows:

– PWM duty cycle (D_{PWM}): 60%, 70%, 80%, 85%, 90%,
– PWM frequency (f_{PWM}): 2 kHz, 4 kHz, 8 kHz, 16 kHz, 40 kHz,
– Load resistance (R_{L}): 200 Ω, 400 Ω, 600 Ω, 800 Ω, 1000 Ω.

For each grid point, the frequency response of the load voltage was measured in the frequency range from 30 Hz to 25 Hz. Table 3 summarizes the maximum power and output voltage values obtained for different acceleration values.

Comparing the results summarized in Table 3 with the maximum values obtained from measurements without the converter, it can be observed that the converter significantly increases the system's output voltage. This makes the generator-converter system practical, as it can achieve a DC voltage of 3.3 V at an acceleration of 5 m/s^2. The downside of this solution is a significant reduction in output power and bandwidth compared to the system without the converter. However, given battery-powered electronic systems' voltage and type requirements, a converter is essential and indispensable in practical applications. Most microcontrollers require a DC supply voltage of 3.3 V, and in energy-saving applications, 1.8 V is sufficient.

Below are detailed maps showing the relationship between output voltage and power as a function of vibration frequency and converter parameters, such as PWM frequency, duty cycle, and load resistance. Four parameter sets were considered (Table 3) for the maximum voltage and power values for accelerations of 5 m/s^2 and 10 m/s^2. Figures 5 and 6 show contour plots

Table 3. Comparison of maximum power and maximum voltage for two different accelerations

Excitation acceleration	**Maximum voltage**	**Maximum power**
5 m/s^2	3.59 V @ vibration frequency – 27.6 Hz, PWM duty – 60%, PWM frequency – 4 kHz, R_L – 1000 Ω), output power – 12.91 mW	15.4 mW @ vibration frequency – 27.9 Hz, PWM duty – 60%, PWM frequency – 4 kHz, R_L – 200 Ω, output voltage – 1.75 V
10 m/s^2	5.32 V @ vibration frequency – 26.1 Hz, PWM duty – 60%, PWM frequency – 4 kHz, R_L – 1000 Ω, output power – 28.34 mW	30.25 mW @ vibration frequency – 26.7 Hz, PWM duty – 70%, PWM frequency – 4 kHz, R_L – 400 Ω, output voltage – 3.48 V

as a function of two variables, with the remaining variables held constant, as in Table 3, for an excitation acceleration of 5 m/s^2 and maximum voltage. The white dashed lines on the voltage and power plots are equipotential lines for voltages of 1.8 V and 3.3 V.

As observed, achieving a voltage above 1.8 V for practically every load resistance value is possible. The bigger the resistance, the higher the voltage, albeit resulting in a power reduction. The highest power and voltage values occur for PWM frequencies in the 2 to 8 kHz range and for PWM duty cycles between 60% and 80%. In this range, an output voltage above 3.3 V can be obtained for load resistances above 850 Ω. Figures 7 and 8 show the results for the operating point of the converter with a maximum power of 15.4 mW, with a vibration frequency, PWM duty cycle, PWM frequency, and R_L of 27.9 Hz, 60%, 4 kHz, and 200 Ω, respectively. The output voltage at the maximum power point is 1.75 V. Unfortunately, when maximizing power, it is impossible to achieve an output voltage above 1.8 V, as shown in the first two rows of Figs. 7 and 8. Measurements for acceleration of 5 m/s^2 show that the converter must operate near the point of maximum voltage, which results in a power reduction compared to the potential maximum power.

Figures 9 and 10 present analogous maps for an acceleration of 10 m/s^2 at the maximum voltage point, while Figs. 11 and 12 show the maps for the maximum power point. Measurements for acceleration of 10 m/s^2 indicate that a minimum voltage of 1.8 V can be achieved across practically the entire range of parameter variations, except in areas where the duty cycle exceeds 85% and the PWM frequency is higher than 10 kHz, for loads not exceeding 400 Ω. Assuming a load of 1000 Ω, corresponding to the maximum voltage point, a minimum voltage of 3.3 V can be achieved over a wide range of parameter variations. This fact enables the application of multi-criteria optimization algorithms in future systems that simultaneously control voltage and output power.

The maps show that the converter's output voltage increases with increased load resistance, which was expected. Interestingly, the highest voltage values were obtained for a PWM frequency of 4 kHz.

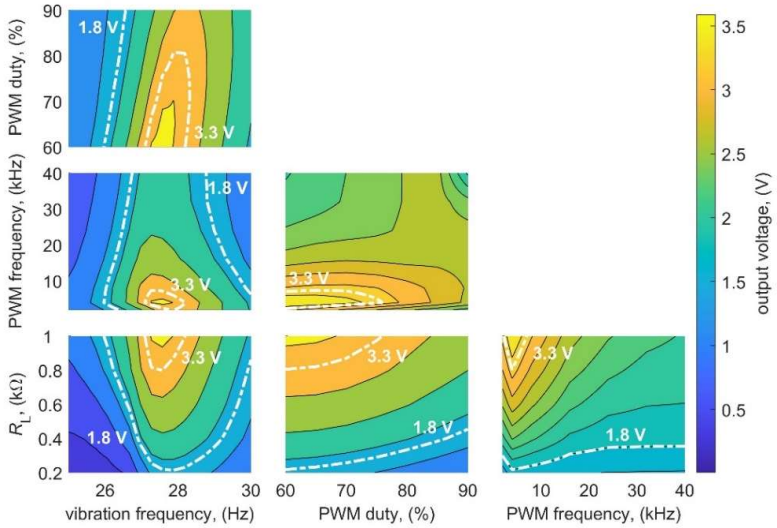

Fig. 5. Performance maps of the output voltage of electromagnetic energy harvester with bridgeless boost rectifier at 5 m/s^2. Each contour plot shows the dependency of output voltage on two variables of the four, with the remaining two variables equal as in Table 3 (vibration frequency – 27.6 Hz, PWM duty – 60%, PWM frequency – 4 kHz, R_L – 1000 Ω)

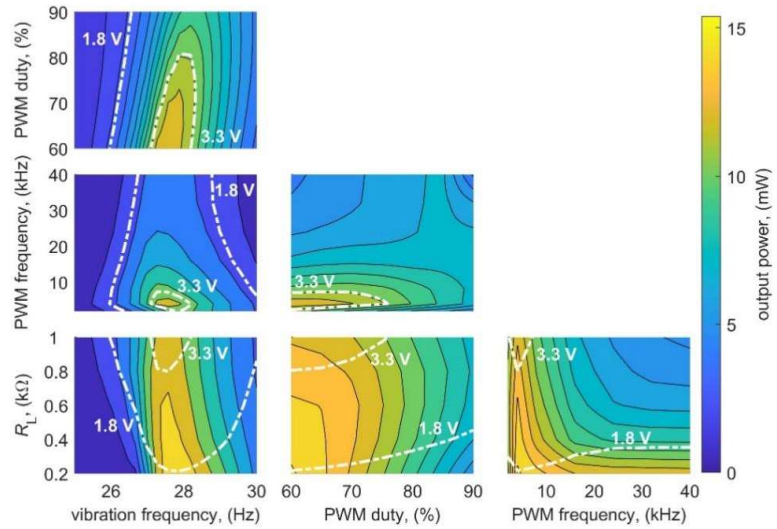

Fig. 6. Performance maps of the output power of electromagnetic energy harvester with bridgeless boost rectifier at 5 m/s^2. Each contour plot shows the dependency of output power on two variables of the four, with the remaining two variables equal as in Table 3 (vibration frequency – 27.6 Hz, PWM duty – 60%, PWM frequency – 4 kHz, R_L – 1000 Ω)

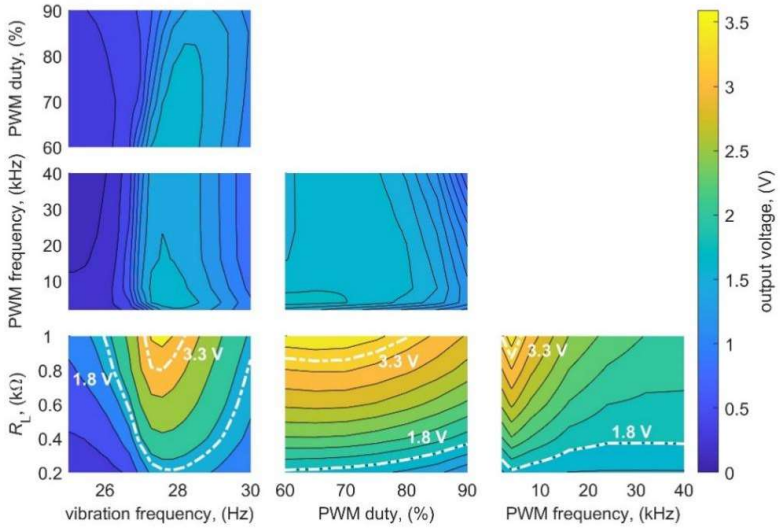

Fig. 7. Performance maps of the output voltage of electromagnetic energy harvester with bridgeless boost rectifier at 5 m/s^2. Each contour plot shows the dependency of output voltage on two variables of the four, with the remaining two variables equal as in Table 3 (vibration frequency – 27.9 Hz, PWM duty – 60%, PWM frequency – 4 kHz, R_L – 200 Ω)

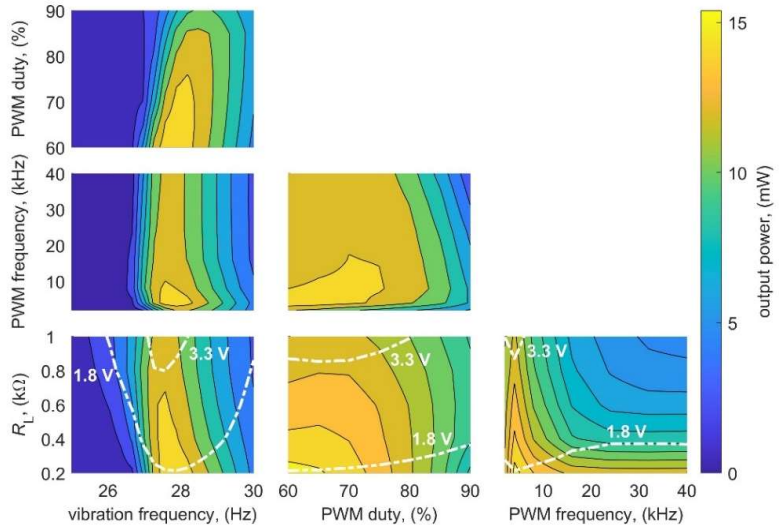

Fig. 8. Performance maps of the output power of electromagnetic energy harvester with bridgeless boost rectifier at 5 m/s^2. Each contour plot shows the dependency of output power on two variables of the four, with the remaining two variables equal as in Table 3 (vibration frequency – 27.9 Hz, PWM duty – 60%, PWM frequency – 4 kHz, R_L – 200 Ω)

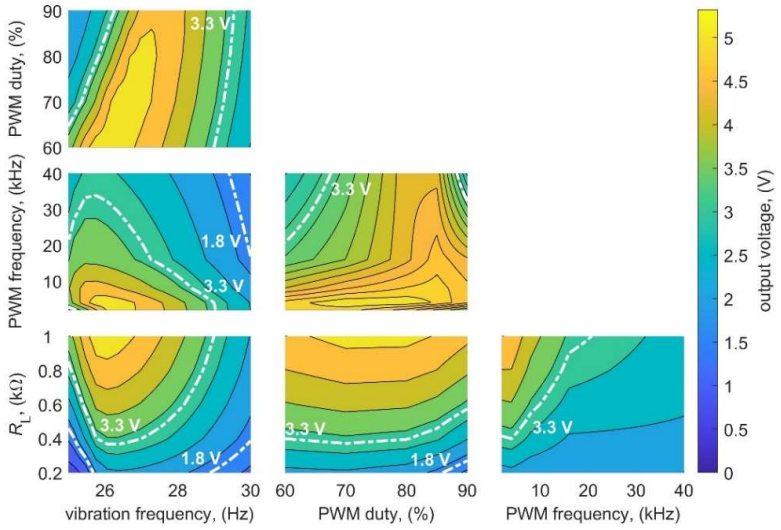

Fig. 9. Performance maps of the output voltage of electromagnetic energy harvester with bridgeless boost rectifier at 10 m/s^2. Each contour plot shows the dependency of output voltage on two variables of the four, with the remaining two variables equal as in Table 3 (vibration frequency – 26.1 Hz, PWM duty – 60%, PWM frequency – 4 kHz, R_L – 1000 Ω)

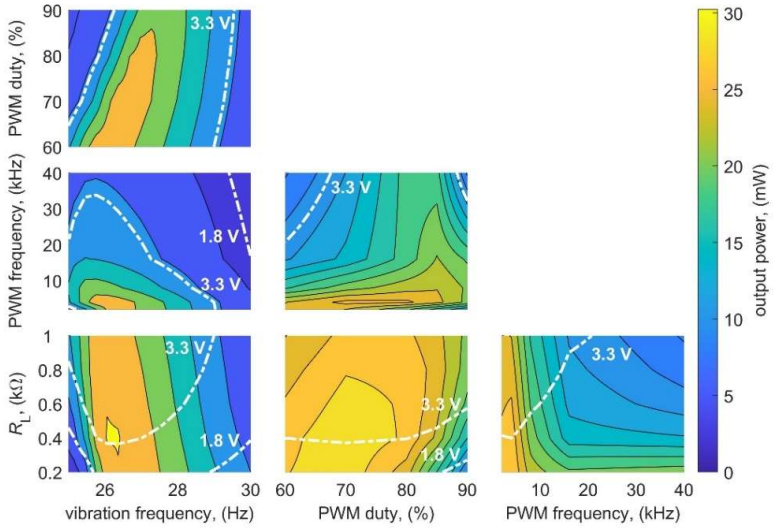

Fig. 10. Performance maps of the output power of electromagnetic energy harvester with bridgeless boost rectifier at 10 m/s^2. Each contour plot shows the dependency of output power on two variables of the four, with the remaining two variables equal as in Table 3 (vibration frequency – 26.1 Hz, PWM duty – 60%, PWM frequency – 4 kHz, R_L – 1000 Ω)

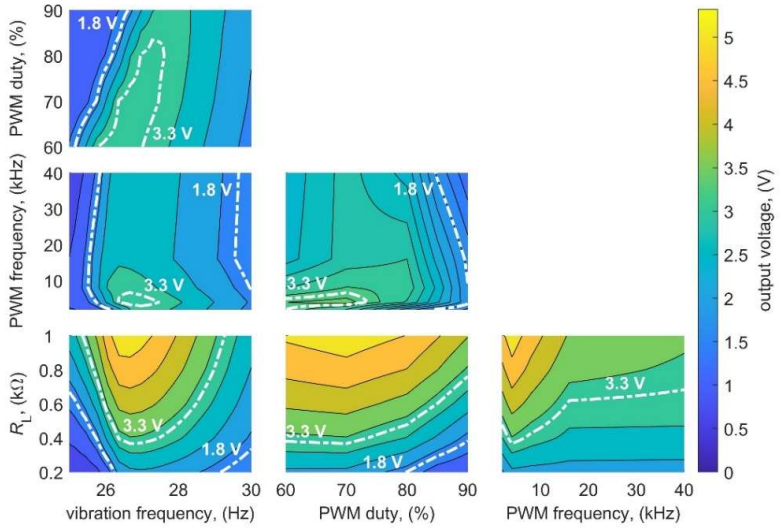

Fig. 11. Performance maps of the output voltage of electromagnetic energy harvester with bridgeless boost rectifier at 10 m/s^2. Each contour plot shows the dependency of output voltage on two variables of the four, with the remaining two variables equal as in Table 3 (vibration frequency – 26.7 Hz, PWM duty – 70%, PWM frequency – 4 kHz, R_L – 400 Ω)

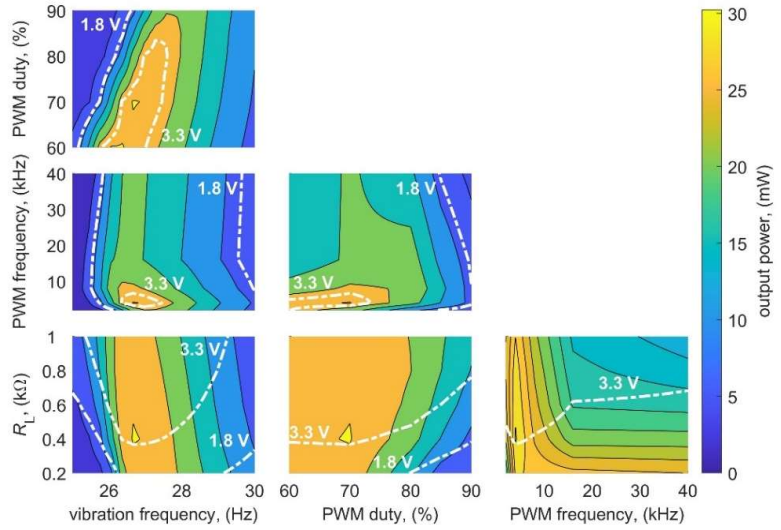

Fig. 12. Performance maps of the output power of electromagnetic energy harvester with bridgeless boost rectifier at 10 m/s^2. Each contour plot shows the dependency of output power on two variables of the four, with the remaining two variables equal as in Table 3 (vibration frequency – 26.7 Hz, PWM duty – 70%, PWM frequency – 4 kHz, R_L – 400 Ω)

The duty cycle significantly affects the resonant frequency. Increasing the PWM frequency shifts the peak voltage and power towards higher frequencies. This time, the load resistance does not significantly impact the bandwidth and resonant frequency as it did in the system without the converter.

The obtained maps allowed for observing the variations of voltage and power depending on the converter parameters. It is evident that in areas with higher voltages (above 3 V), there is a slight decrease in output power relative to the maximum power. For an acceleration of 5 m/s^2, the converter's operating point should oscillate around the maximum voltage point for applications requiring both 3.3 V and 1.8 V. At an acceleration of 10 m/s^2, it is readily possible to optimize both voltage and power simultaneously, especially for applications requiring 1.8 V.

4. Conclusions

The research conducted in this study has led to several significant accomplishments that advance the understanding and application of nonlinear electromagnetic vibration energy harvesters. The achievements of general significance are:

- New zero-crossing detection circuit using a comparator with input and output filters to enhance accuracy and reduce noise.
- A detailed investigation of the converter's performance as a nonlinear system without simplifications and assumptions examining the impact of converter operation and loading on the bandwidth.

The findings of the research on this specific tri-stable electromagnetic energy harvester with a bridgeless boost rectifier are as outlined below:

- Determination of the impact of generator parameters and vibration frequency on the output power and voltage: Explored the influence of various converter parameters and vibration frequencies on output voltage and power, offering valuable insights for selecting appropriate regulators in future applications.
- Identification of optimal operating regions: Delineated operating regions where the converter can achieve required voltage levels (1.8 V, 3.3 V) with relatively high output power, rendering it applicable for diverse practical scenarios.
- Foundation for a future dual generator and converter system: The research establishes the groundwork for developing a dual generator, encompassing tri-stable and bi-stable harvesters and a converter system. This paves the way for even more advanced energy harvesting systems.

References

[1] Wang W., Li B., Wang J., Fang B., Li Z., Liu S., Wei R., *Harnessing energy from hand-shaking vibration for electronics through a magnetic rolling pendulum bistable energy harvester*, Energy Conversion and Management, vol. 310, no. 1, 118466 (2024), DOI: 10.1016/j.enconman.2024.118466.

[2] Lo Monaco M., Russo C., SomaÌ A., *Numerical and experimental performance study of two-degrees-of-freedom electromagnetic energy harvesters*, Energy Conversion and Management: X, vol. 18, no. 1, 100348 (2023), DOI: 10.1016/j.ecmx.2023.100348.

[3] Maamer B., Jaziri N., Hadj Said M., Tounsi F., *High-displacement electret-based energy harvesting system for powering leadless pacemakers from heartbeats*, Archives of Electrical Engineering, vol. 72, no. 1, pp. 229–238 (2023), DOI: 10.24425/aee.2023.143699.

[4] Ostrowski M., Błachowski B., Bocheński M., Piernikarski D., Filipek P., Janicki W., *Design of nonlinear electromagnetic energy harvester equipped with mechanical amplifier and spring bumpers*, Bulletin of the Polish Academy of Sciences: Technical Sciences, vol. 68, no. 6, pp. 1373–1383 (2020), DOI: 10.24425/bpasts.2020.135384.

[5] Mitura A., Kecik K., *Modeling and energy recovery from a system with two pseudo-levitating magnets*, Bulletin of the Polish Academy of Sciences: Technical Sciences, vol. 70, no. 4, 141721 (2022), DOI: 10.24425/bpasts.2022.141721.

[6] Li X., Huang K., Li Z., Xiang J., Huang Z., Mao H., Cao Y., *Investigation of the influence of additional magnets positions on four-magnet bi-stable piezoelectric energy harvester*, Bulletin of the Polish Academy of Sciences: Technical Sciences, vol. 70, no. 1, 140151 (2022), DOI: 10.24425/bpasts.2022.140151.

[7] Jiang Q., Yu C., Zhou Y., Zhao Z., Gao Q., Sun B., *Modeling and analysis of beam-spring magnetically coupled bistable energy harvester for broadband vibration energy harvesting*, Journal of Sound and Vibration, vol. 579, no. 1, 118373 (2024), DOI: 10.1016/j.jsv.2024.118373.

[8] Zeng Z., Ren B., Xu Q., Lin D., Di W., Luo H., Wang D., *Excellent performances of energy harvester using cantilever driving double-clamped 0.7Pb(Mg1/3Nb2/3)O3-0.3PbTiO3 plates and symmetric middle-stops*, Applied Physics Letters, vol. 107, no. 17, 173502 (2015), DOI: 10.1063/1.4934700.

[9] Zhang J., Zhi Y., Yang K., Hu N., Peng Y., Wang B., *Internal resonance characteristics of a bistable electromagnetic energy harvester for performance enhancement*, Mechanical Systems and Signal Processing, vol. 209, no. 1, 111136 (2024), DOI: 10.1016/j.ymssp.2024.111136.

[10] Thainiramit P., Yingyong P., Isarakorn D., *Impact-Driven Energy Harvesting: Piezoelectric Versus Triboelectric Energy Harvesters*, Sensors, vol. 20, no. 20, 5828 (2020), DOI: 10.3390/s20205828.

[11] Li X., Yurchenko D., Li R., Feng X., Yan B., Yang K., *Performance and dynamics of a novel bistable vibration energy harvester with appended nonlinear elastic boundary*, Mechanical Systems and Signal Processing, vol. 185, no. 1, 109787 (2023), DOI: 10.1016/j.ymssp.2022.109787.

[12] Zhou S., Cao J., Inman D.J., Lin J., Liu S., Wang Z., *Broadband Tristable Energy Harvester: Modeling and Experiment Verification*, Appl. Energy, vol. 133, pp. 33–39 (2014), DOI: 10.1016/j.apenergy.2014.07.077.

[13] Zhou S., Zuo L., *Nonlinear Dynamic Analysis of Asymmetric Tristable Energy Harvesters for Enhanced Energy Harvesting*, Commun. Nonlinear Sci. Numer. Simul., vol. 61, pp. 271–284 (2018), DOI: 10.1016/j.cnsns.2018.02.017.

[14] Litak G., Margielewicz J., Gąska D., Wolszczak P., Zhou S., *Multiple Solutions of the Tristable Energy Harvester*, Energies, vol. 14, 1284 (2021), DOI: 10.3390/en14051284.

[15] Xu J., Leng Y., Sun F., Su X., Chen X., *Modeling and Performance Evaluation of a Bi-Stable Electromagnetic Energy Harvester with Tri-Magnet Levitation Structure*, Sensors Actuators A Phys., vol. 346, 113828 (2022), DOI: 10.1016/j.sna.2022.113828.

[16] Kashiwao T., Izadgoshasb I., Lim Y.Y., Deguchi M., *Optimization of rectifier circuits for a vibration energy harvesting system using a macro-fiber composite piezoelectric element*, Microelectronics Journal, vol. 54, pp. 109–115 (2016), DOI: 10.1016/j.mejo.2016.05.013.

[17] Clemente C.S., Iannone I., Loschiavo V.P., Davino D., *Design and Optimization of a Boost Interface for Magnetostrictive Energy Harvesting*, Applied Sciences, vol. 13, no. 3, 1606 (2023), DOI: 10.3390/app13031606.

[18] Potocny M., Kovac M., Arbet D., Sovcik M., Nagy L., Stopjakova V., Ravasz R., *Low-Voltage DC-DC Converter for IoT and On-Chip Energy Harvester Applications*, Sensors, vol. 21, no. 17, 5721 (2021), DOI: 10.3390/s21175721.

[19] Yang Z., Zhang Y., Li Z., Zhang Z., Fu L., Kan J., *Design and characteristic analysis of a high-performance deformable piezoelectric wind energy harvester based on coupled vibrations*, Sustainable Materials and Technologies, vol. 42 (2024), DOI: 10.1016/j.susmat.2024.e01134.

[20] Sutikno T., Subrata A.C., Pau G., Jusoh A., Ishaque K., *Maximum power point tracking techniques for low-cost solar photovoltaic applications*, Archives of Electrical Engineering, vol. 72, no. 2, pp. 299–322 (2023), DOI: 10.24425/aee.2023.145410.

[21] Dayal R., Parsa L., *A New Single Stage AC–DC Converter for Low Voltage Electromagnetic Energy Harvesting*, 2010 IEEE Energy Convers. Congr. Expo. ECCE 2010 - Proc., pp. 4447–4452 (2010), DOI: 10.1109/ECCE.2010.5618446.

[22] Mitcheson P.D., Green T.C., Yeatman E.M., *Power Processing Circuits for Electromagnetic, Electrostatic and Piezoelectric Inertial Energy Scavengers*, Microsyst. Technol., vol. 13, pp. 1629–1635 (2007), DOI: 10.1007/s00542-006-0339-0.

[23] Cao X., Chiang W.J., King Y.C., Lee Y.K., *Electromagnetic Energy Harvesting Circuit with Feedforward and Feedback Dc-Dc PWM Boost Converter for Vibration Power Generator System*, IEEE Trans. Power Electron., vol. 22, pp. 679–685 (2007), DOI: 10.1109/TPEL.2006.890009.

[24] Lefeuvre E., Audigier D., Richard C., Guyomar D., *Buck-Boost Converter for Sensorless Power Optimization of Piezoelectric Energy Harvester*, IEEE Trans. Power Electron., vol. 22, pp. 2018–2025 (2007), DOI: 10.1109/TPEL.2007.904230.

[25] Tang Y., Khaligh A., *A Multiinput Bridgeless Resonant AC–DC Converter for Electromagnetic Energy Harvesting*, IEEE Trans. Power Electron., vol. 31, pp. 2254–2263 (2013), DOI: 10.1109/TPEL.2015.2426700.

[26] Wang H., Tang Y., Khaligh A., *A Bridgeless Boost Rectifier for Low-Voltage Energy Harvesting Applications*, IEEE Trans. Power Electron., vol. 28, pp. 5206–5214 (2013), DOI: 10.1109/TPEL.2013.2242903.

[27] Kwon D., Rincon-Mora G.A., *A rectifier-free piezoelectric energy harvester circuit*, Proc. IEEE International Symp. Circuits Syst., Taipei, Taiwan, pp. 1085–1088 (2009), DOI: 10.1109/ISCAS.2009.5117948.

[28] Jagieła M., Kulik M., *Wideband Electromagnetic Converter of Mechanical Vibrations Energy into Electrical Energy* (in Polish), Patent Office of the Republic of Poland, No. Pat. 239301 (2017).

[29] Kulik M., Jagieła M., Łukaniszyn M., *Surrogacy-based maximization of the output power of a low-voltage vibration energy harvesting device*, Applied Sciences, vol. 10, no. 7, 2484 (2020), DOI: 10.3390/APP10072484.

[30] Kulik M., Górecki K., Jagieła M., *Impact of scale factor on performance of miniature DC power source based on wideband vibration energy converter*, Przegląd Elektrotechniczny, vol. 98, no. 8, pp. 185–188 (2022), DOI: 10.15199/48.2022.08.34.